Temperature-dependency of hysteretic sorption in hygrothermal modelling of wood fibreboard sheathing: analysis of exterior wall laboratory experiments

Petteri Huttunen & Juha Vinha

Published online: 27 Dec 2023.

Submit your article to this journal ↗

Article views: 84

View related articles ↗

View Crossmark data ↗

Temperature-dependency of hysteretic sorption in hygrothermal modelling of wood fibreboard sheathing: analysis of exterior wall laboratory experiments

Petteri Huttunen and Juha Vinha

Faculty of Built Environment, Tampere University, Tampere, Finland

ABSTRACT

Wood is known for its temperature-dependent and hysteretic sorption behaviour. Several hysteresis models can be found from the literature, but the temperature-dependency of sorption especially in cold temperatures has received less attention. In this paper, we show experimental results for low-density fibreboard, which can be obtained with relatively inexpensive equipment and used for constructing temperature-dependent EMC function. The results were applied in the numerical analyses of a previous laboratory experiment involving an exterior wall with an LDF layer as sheathing. The optimal parameters for hysteresis models were determined by the least-squares data fitting approach. Our conclusion is that both the temperature-dependency and hysteresis in sorption behaviour must be included and with proper model parameters in the hygrothermal model in order to obtain satisfactory results when modelling LDF sheathing in a cold climate. Existing literature related to these aspects in hygrothermal modelling is scarce, and more experimental and computational research is needed.

1. Introduction

Computational analyses of combined heat and moisture transport are a significant part of modern hygrothermal design of building envelopes and building physical research. Useful approximations of time-dependent temperature and moisture distributions inside building envelope assemblies under the influence of different weather and indoor conditions can be obtained by numerical solutions of hygrothermal models, which are based on conservation equations of energy and mass inside porous material. An adequate hygrothermal model should include all the significant mechanisms related to moisture storage and transfer, but the significance of the different known physical phenomena of moisture is very material specific. Wood and wood-based materials such as fibreboards are examples of materials that are known to exhibit significant hysteretic and temperature-dependent behaviour regarding moisture sorption in the hygroscopic range (Dinwoodie 2000; Skaar 1988). Available software for numerical building physical analyses rarely include built-in capability for modelling these phenomena and the advanced numerical studies related to this topic, such as Lelievre, Colinart, and Glouannec (2014), Rahim et al. (2016) and Zhang et al. (2016), have to rely on specifically created codes or multipurpose physics simulation software where custom models can be defined. Moreover,

as observed by Zhang et al. (2016), the subject of combined effect of hysteresis and temperature-depenency of sorption has not received much focus in building physical research. The authors stated that they were aware of only two papers which 'attempted to study the combined effect of temperature-dependent sorption and sorption hysteresis for hygrothermal modeling' and referred to Rode and Clorius (2004) and Frandsen (2007).

In this paper we examine a previous laboratory experiment involving an exterior wall. Previous numerical analyses related to this experiment have shown an unsatisfactory agreement between measurements inside similar structures and the corresponding modelling results. In this paper, we use a more sophisticated hygrothermal model than conventional one, where the hysteresis and temperature-dependence of sorption are both applied by utilizing the method for modelling hysteresis as presented in Rode and Clorius (2004) and Frandsen (2007). However, novel material measurements were carried out in order to obtain the necessary data related to the temperature-dependence of sorption with a wide temperature range – including cold temperatures i.e. $-20 \ldots 0°C$ – in low-density fibreboard (LDF, 280 kg/m³), which was used in the sheathing of the examined structure. The results are analysed by comparing them to conventional modelling, where only a single sorption curve

---

is used without temperature dependence. Finally, we discuss the state-of-the-art in related hygrothermal modelling and the significance of these phenomena in long-term numerical analyses.

2. Materials and methods

2.1. Hygrothermal models

Currently, the conventional and typical way of modelling combined heat and moisture transport in building envelope structures relies on the following equations for conservation of heat and mass (Künzel 1995):

$$(\rho C_p)_{\text{eff}} \frac{\partial T}{\partial t} = \nabla \cdot (\lambda \nabla T + h_v \delta_p \nabla (\varphi p_{\text{sat}})) \quad (1)$$

$$\frac{\partial w}{\partial t} = \xi \frac{\partial \varphi}{\partial t} = \nabla \cdot (\xi D_w \nabla \varphi + \delta_p \nabla (\varphi p_{\text{sat}})) \quad (2)$$

where:

$$(\rho C_p)_{\text{eff}} = (w(\varphi) C_{p,\text{water}} + \rho_{\text{dry}} C_{p,\text{dry}}) \quad (3)$$

$$\xi = \frac{\partial w(\varphi)}{\partial \varphi} \quad (4)$$

The differential moisture capacity, ξ, is the humidity-dependent mass coefficient in Equation (2), which can be computed from either the adsorption or desorption isotherm or from their average. Determination of sorption isotherms is typically carried out by the gravimetric method, where material samples are conditioned in a desiccator or climatic chamber and weighed repeatedly until equilibrium is reached (ISO 12571:2021). However, this procedure is problematic in cold temperatures due to e.g. the difficulties involved in controlling air humidity accurately in cold temperatures. Consequently, not much temperature-dependent sorption data in cold temperatures for different building materials is widely available. With the temperature-dependency included, the left-hand side of Equation (2) should have the following terms, for which we use the following subscript notation:

$$\frac{\partial w(\varphi, T)}{\partial \varphi} = \rho_{\text{dry}} \left(\frac{\partial u}{\partial \varphi} \cdot \frac{\partial \varphi}{\partial t} + \frac{\partial u}{\partial T} \cdot \frac{\partial T}{\partial t} \right)$$

$$= \rho_{\text{dry}} \left(\xi_\varphi(\varphi, u, T) \frac{\partial \varphi}{\partial t} + \xi_T(\varphi, u, T) \frac{\partial T}{\partial t} \right) \quad (5)$$

We applied the hysteresis model introduced originally by Rode, Hansen, and Hansen (1990) and generalized by Frandsen (2007), where the ξ_φ depends on the direction of the sorption process:

$$\xi_\varphi = \begin{cases} \dfrac{A \cdot (u - u_a)^B \xi_d + (u_d - u)^B \xi_a}{(u_d - u_a)^B}, & \frac{\partial \varphi}{\partial t} \geq 0 \\[3mm] \dfrac{(u - u_a)^B \xi_d + A \cdot (u_d - u)^B \xi_a}{(u_d - u_a)^B}, & \frac{\partial \varphi}{\partial t} < 0 \end{cases} \quad (6)$$

where u_a and u_d are the moisture contents in equilibrium according to either the adsorption or desorption curve at current relative humidity. Likewise, ξ_a and ξ_d are the differential moisture capacities computed from either the adsorption or desorption curve. Parameters A and B originally had values 0.1 and 2.0 (Rode, Hansen, and Hansen 1990), respectively, but more precise species-specific values can be used if they are obtained by data fitting from experimental data (Carmeliet, De Wit, and Janssen 2005; Frandsen 2007). In this paper we use both the original model and the generalized model, but also extend the generalized model by using different parameter values for the adsorption and desorption processes: A_{up}, B_{up} (when $\partial \varphi / \partial t \geq 0$) and A_{down}, B_{down} (when $\partial \varphi / \partial t < 0$). Optimal parameter values are obtained via least-squares fitting, which is described in a later chapter.

2.2. Determination of temperature-dependency of sorption

At first, a commercially manufactured dynamic vapour sorption (DVS) analyser was used to determine adsorption and desorption curves at 20°C. The sample sizes (dry weights) were 11 and 26 mg, and the equilibration time between RH steps was 30 h. The measured adsorption and desorption data is presented in Table 1. A photograph of the used DVS system is shown in Figure 1 (left). The dry density of the material is 280 kg/m³. The determination of desorption curve is started by wetting the sample with liquid water instead of equilibrating the sample with RH close to 100% RH, as it should be done according to Fredriksson and Thybring (2018). When applying in further calculations the results of DVS analyses carried out by using small samples, one should be aware of that there is some variation in the actual pore volumes between different samples and this has some effect on equilibrium moisture contents (EMC) at very high humidities where moisture is also present in liquid form in the pores. For wooden materials such as the studied LDF, we assume that the amount of liquid water is zero when the humidity is below fibre saturation point of wood, which we assume to be over 28% in moisture content per dry mass, i.e. clearly above 95% RH.

A set of test tubes was filled with LDF samples and humidity probes in order to obtain data of the temperature-dependence in moisture capacity (Vaisala HMP100) (see: Figure 1, right; and Figure 2). The small samples detached with a knife from the intact LDF board were initially fully wet. They were then dried in room temperature, with the drying time ranging from less than one hour to a few hours in order to get samples with varying moisture contents. Ultimately, nine test tubes where initial moisture contents corresponded with
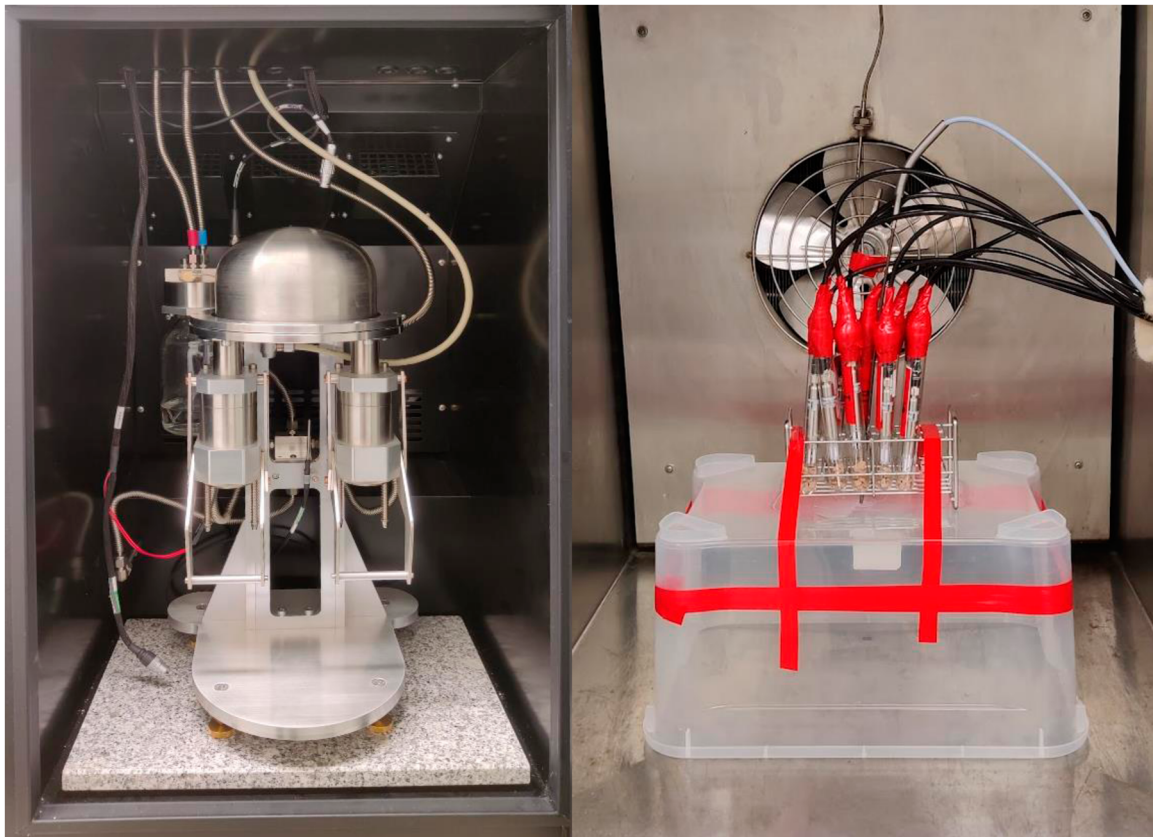
Figure 1. Photographs of the used test equipment: DVS sorption balance (left) and temperature chamber with test tubes (right).

Table 1. Tabulated values for LDF adsorption and desorption isotherms (20°C) measured with the DVS system.

φ [-]	0	0.19	0.29	0.39	0.49	0.54	0.59	0.64	0.69	0.74	0.77	0.80
u_{ads} [kg/kg]	0	0.049	0.056	0.064	0.073	0.078	0.084	0.092	0.103	0.116	0.125	0.132
φ [-]	0.82	0.85	0.87	0.90	0.92	0.95	0.97					
u_{ads} [kg/kg]	0.141	0.151	0.163	0.178	0.199	0.229	0.279					
φ [-]	0	0.19	0.29	0.39	0.49	0.59	0.65	0.70	0.75	0.80	0.85	0.90
u_{des} [kg/kg]	0	0.054	0.072	0.088	0.105	0.125	0.136	0.149	0.163	0.181	0.204	0.241

relative humidities from 52% RH to 99% RH in room temperature were obtained. The tubes were sealed with sticker mass and plastic tape. They were then placed in a temperature chamber and conditioned in different temperatures (at least 8 h) in descending order from the initial temperature (from 20°C to −22°C). Because the moisture capacity of wood increases when the temperature drops, the readings from the humidity probes will also drop because the total amount of moisture in a sealed tube is constant regardless of the temperature change. With this experiment we get data points of the sample material's temperature-dependent equilibrium moisture content function. We can then use the data points for constructing a dense data table of EMC at different temperatures and relative humidities, which can then be used by numerical software to get the necessary values of EMC in an arbitrary point of (T, φ)-space by interpolation. A photograph of the temperature chamber test setup is shown

in Figure 1 (right). A pt100 sensor was used to measure the temperature in the chamber.

The results of the test tube measurements in the temperature chamber are shown in Table 2. For the measurements of each tube, a second-order polynomial fit is drawn for $\varphi(T)$ (exception: fourth-order polynomial fit for tube 2) and the polynomials are drawn in Figure 3 (except for tube 1). Interestingly, the readings from the two tubes with the highest initial humidity fall steeply when the temperature falls to the range of −15 … −20°C, and tube 1, with the highest moisture content, shows lower relative humidity at −22.0°C than tube 2. This inconsistency is most likely caused by the humidity probes' behaviour at cold temperatures, where the accuracy of the probe starts to suffer, particularly when in very humid conditions. The uncertainty for the capacitive humidity probes declared by the manufacturer (± 3.0% RH at −40 … 0°C and 0 … 90% RH) is greater than the difference between

Figure 2. Test tube with LDF material in small pieces and humidity probe.
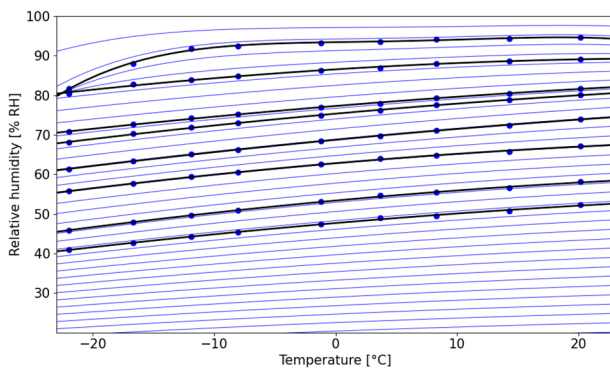

Figure 3. Visualized results from the test tube measurements and polynomial fits (black lines). Blue lines are examples of approximation lines.

two readings from one tube in consecutive temperatures, but we assume that the systemic error is almost the same for the same probe in two consecutive conditions, which – in this case – have always less than 6°C difference in temperature and less than 2% RH difference on average in relative humidity. This means that the accuracy of measuring the difference of relative humidity between two conditions is much better than the absolute uncertainty of a single reading, and capacitive probes such as Vaisala HMP110 can be meaningfully used to record the temperature-dependent data, like in this study.

Once the polynomial fits are calculated for the test tubes, we can draw arbitrarily many approximation lines in the coordinate system of Figure 3 by choosing any initial point in the adsorption or desorption curve (at 20°C) and use the neighbouring polynomial fits to compute new constant mass line (blue lines in Figure 3) as weighted average of the two neighbouring polynomials. Below the driest tube's line (tube 9), we used flat line $\varphi(T) = 0$ as the other neighbouring line. With this principle, a large set of initial data for both adsorption and

desorption isotherms at temperatures $-20 \ldots 20°C$ was generated with a Python script, the output of which was used in the laboratory test wall simulations.

2.3. Laboratory test wall setup and simulation details

Different hygrothermal models were applied to again analyse numerically one of the several laboratory test wall experiments reported in Vinha (2007: Appendix 1). Some of these test walls, which had wood fibreboard sheathing, have been previously numerically analysed in Kalamees and Vinha (2003) and Laukkarinen and Vinha (2011) without a satisfactory agreement between numerical results and measurements of RH behind the sheathing. The equipment used in the experiment is based on a calibrated hot-box-type warm chamber located inside the freezer room. One of the warm chamber's sides has an opening for the test element (approx. 1200 mm × 1200 mm), which can be any vertical building envelope part, such as an exterior wall or window. The warm chamber and the protective chamber around the test wall contain the required devices for adjusting temperatures and humidities. During the early 2000s, the equipment was used to experimentally analyse several different exterior wall types, and more detailed information related to the equipment can be found in Vinha (2007). The test had three consecutive phases simulating the conditions of autumn, winter and spring. Illustrations of the equipment and the test programme consisting of three phases are shown in Figure 4.

In this paper, we analyze one test assembly, that was divided into four segments (542 mm × 542 mm) and two of those segments had the following material layers (from inside to outside):

- Gypsum board, 13 mm
- Plastic vapour retarder membrane ($S_d = 100$ m)
- Glass wool insulation, 173 mm
- LDF sheathing board, 25 mm
- Air gap 25 mm
- Façade boarding

Both segments were thus subjected to the same conditions at the interior and exterior surfaces. The difference between the two segments, however, was that before the experiment the materials used in different sides were equilibrated in different relative humidities before construction, see Appendix 2 of Vinha (2007) and wall types 1a and 1b. The materials were conditioned in 55% RH and 86% RH, but they dried to some extent during the construction process. For the initial relative humidity in the computations, we used 50% RH and 74% RH, which

Table 2. Tabulated results (relative humidity, % RH and pt100 reference temperature readings, °C) from the test tube measurements.

T [°C]	Tube 1	Tube 2	Tube 3	Tube 4	Tube 5	Tube 6	Tube 7	Tube 8	Tube 9
20.2	99.5	94.6	89.2	81.7	80.1	73.9	67.2	58.1	52.3
14.3	99.9	94.3	88.6	80.5	78.8	72.4	65.8	56.6	50.7
8.3	100.2	94.1	88.0	79.4	77.6	71.1	64.7	55.4	49.5
3.7	100.4	93.5	86.9	77.9	76.1	69.8	63.9	54.6	49.0
−1.2	100.3	93.3	86.3	77.0	75.0	68.4	62.5	53.1	47.4
−8.0	94.2	92.5	84.9	75.2	73.0	66.2	60.5	50.9	45.4
−11.9	90.4	91.8	84.0	74.2	71.9	65.1	59.4	49.7	44.3
−16.7	85.8	88.0	82.7	72.7	70.3	63.4	57.7	47.9	42.7
−22.0	80.8	81.7	80.5	70.7	68.1	61.3	55.7	45.9	40.9
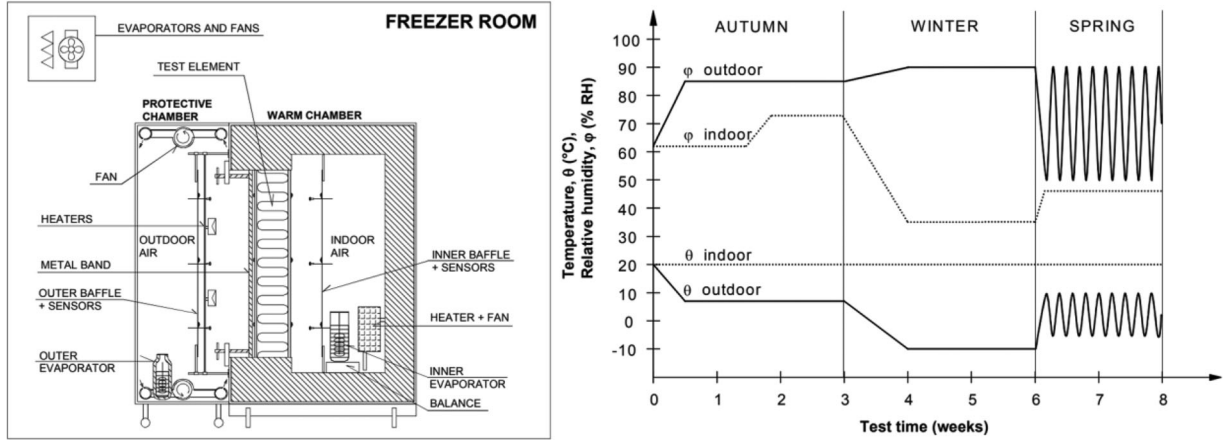
Figure 4. Illustration of the building physical test equipment (left) and the test programme conditions (right) (© Vinha 2007).

were the first measured values in the beginning of the experiment. Here, we also refer with 1a to the segment of the structure with 50% RH initial relative humidity in the materials and with 1b to the segment with 74% RH corresponding initial humidity. Except for the new sorption and temperature-dependence measurements for LDF, the same material properties were used in simulations as in Kalamees and Vinha (2003). The μ-value of LDF is 4.6 (see Appendix 3 of Vinha 2007; material 'A2 Wood fibre-board 25 mm'). Liquid water transport was assumed to be negligible and D_w was set to zero because the humidity didn't exceed 80% RH in the experiment. Boundary conditions were modelled in an identical way where Dirichlet conditions were set on the sheathing surfaces, i.e. the air gap and façade boarding were not modelled. Surface temperatures were measured on the sheathing board, and relative humidity on the surface was computed by using saturation vapour pressure according to surface temperature and partial vapour pressure measured from the air gap.

Simulations were carried out with one-dimensional geometries by using Comsol Multiphysics version 6.1. The LDF layer was modelled by using the software's *Coefficient form PDE* -module where the governing equations can be defined by the user with the hysteretic and temperature-dependent capacity coefficients among other heat and moisture flux terms. Moisture content u is included by

utilizing the software's *state variable* functionality, where the state variable is not part of the solution but can be repeatedly updated by the changing solution at different time steps. The unknown variables T and φ are solved for step $i+1$ by using u from the previous step i, and after the solution the u is updated by:

$$u_{i+1} = u_i + \xi_\varphi(\varphi_{i+1}, u_i, T_{i+1})\varphi_{t,i+1}\Delta t$$
$$+ \xi_T(\varphi_{i+1}, u_i, T_{i+1})T_{t,i+1}\Delta t \quad (7)$$

The temperature derivative term of the moisture capacity, ξ_T, is assumed to behave identically in adsorption and desorption processes, i.e. when $\partial\varphi/\partial t < 0$ and $\partial\varphi/\partial t \geq 0$. The ξ_T is computed as the weighted average of $\partial u_a(\varphi, T)/\partial T$ and $\partial u_d(\varphi, T)/\partial T$, giving more weight to the primary sorption isotherm (adsorption or desorption), which is closer to the current state of moisture:

$$\xi_T = \frac{\partial u_a(\varphi, T)}{\partial T}(1-\theta) + \frac{\partial u_d(\varphi, T)}{\partial T}\theta \quad (8)$$

where:

$$\theta = \frac{u - u_a(\varphi, T)}{u_d(\varphi, T) - u_a(\varphi, T)} \quad (9)$$

The derivatives are computed numerically by interpolation from the data tables of $u_a(\varphi, T)$ and $u_d(\varphi, T)$, created by the steps described in previous chapter and using resolution of 1% RH and 1°C. The software in question

can handle automatically structured or unstructured data sets with 1–3 arguments to create a callable interpolation function, which treats the input data in the same way as linear element mesh (Comsol 2023). Other material layers than LDF were modelled with the software's built-in *Building Materials* -module. Time-stepping by backwards differentiation formulae was set to the order of 1 to ensure that the state variable *u* update by Equation (7) is valid. For every time-step the step size is determined by the software's built-in algorithm, but the maximum step was restricted to one hour. The number of 1D elements (with linear spatial discretization) from every material layer was 120 in total.

The computation of one case of the 736–hour experiment with a temperature-dependent and hysteretic model took around three minutes on average with a desktop PC. A high-performance cluster was used to compute the vast number of cases, utilizing parallelization to find the optimal values of hysteresis model parameters when using the generalized and extended hysteresis model. The reference point (RP) in the comparison of laboratory measurements and simulation results is the interface between the sheathing and the thermal insulation layer, where T/RH-probes (Vaisala HMP 233) were installed inside the test assemblies. For every case of different parameters (1a only), the squared L_2-norm measuring the discrepancy between measurements and simulation was computed from the values related to the RP ($n = 736$):

$$\varepsilon_{L2} = \sum_{t=0}^{n} (\varphi_{meas}(t) - \varphi_{model}(t))^2 \qquad (10)$$

In the sense of grid search optimization, the best values for the generalized and extended hysteresis model were searched from all combinations of the following parameter sets:

- Generalized hysteresis model: A = {0.1, 0.2, 0.3, … , 1.5} ∧ B = {1.5, 1.6, 1.7, … , 3.5}
- Extended hysteresis model:
  - A_{up} = {0.1, 0.2, 0.3, … , 1.5} ∧ A_{down} = {0.1, 0.2, 0.3, … , 1.5}
  - B_{up} = {1.5, 1.6, 1.7, … , 3.5} ∧ B_{down} = {1.5, 1.6, 1.7, … , 3.5}

The ε_{L2} was computed by using relative humidity values in dimensionless units.

3. Results

For the generalized model, the best fit against the data from 1a was obtained by using parameter values: A = 0.9

Table 3. Squared error norms (ε_{L2}, see Equation 10) for test walls 1a and 1b with different models.

	1a	1b
Extended hysteresis model	0.501	0.836
Generalized hysteresis model	0.513	0.960
Original hysteresis model	1.571	1.483
Conventional model	1.360	0.949

and B = 3.3. For the extended model, the best fit was: A_{up} = 0.4, B_{up} = 2.1, A_{down} = 0.9 and B_{down} = 3.0. The comparison of measurements and simulation results from 1a and 1 b using the different hygrothermal models are shown in Figures 5 and 6. By conventional model, we refer to a model where no effects of hysteresis or temperature-dependency are taken into account and the sorption isotherm of LDF used in the simulation is the average between adsorption and desorption curves (see Table 1). T-D refers to temperature-dependence of sorption. The relative humidity conditions at the boundaries of the models are shown in Figure 7.

We can see from Figures 5 and 6 that the agreement between modelling and measurement is visibly best with the generalized and extended hysteresis models with T-D for both cases, 1a and 1b. The level of diurnal variation of RH in RP is of the same magnitude in the spring phase when using the hysteresis model with original parameters, but the overall agreement is somewhat worse in the middle of the experiment, i.e. the winter phase. For segment 1b, the shape of the RH curve from the original hysteresis model with T-D is visibly quite good compared to the measurements, but the squared error norm is higher than that of the conventional model (see Table 3). In this case the conventional model yields a curve which in general is close to the measurements, but the conventional model fails to predict the quick changes during the experiment.

Figure 8 shows the comparison of measured and simulated temperatures in the same point. The simulated temperatures are approximately 1–2°C colder than the measurements taken through the experiment. This is likely due to the inaccuracies in the thermal conductivities used, but the lateral heat flows in the test walls, which are not one-dimensional objects in reality, are also a possible cause. Hysteresis or temperature-dependence in the LDF properties seems to have a negligible effect on the accuracy of simulated temperatures, at least in these test assemblies.

The moisture contents in the reference point according to the different models are compared in Figures 9 and 10. In the conventional model the initial moisture content is larger than in others because the average of adsorption and desorption curves was used in the computation. In hysteretic models, the initial moisture content was
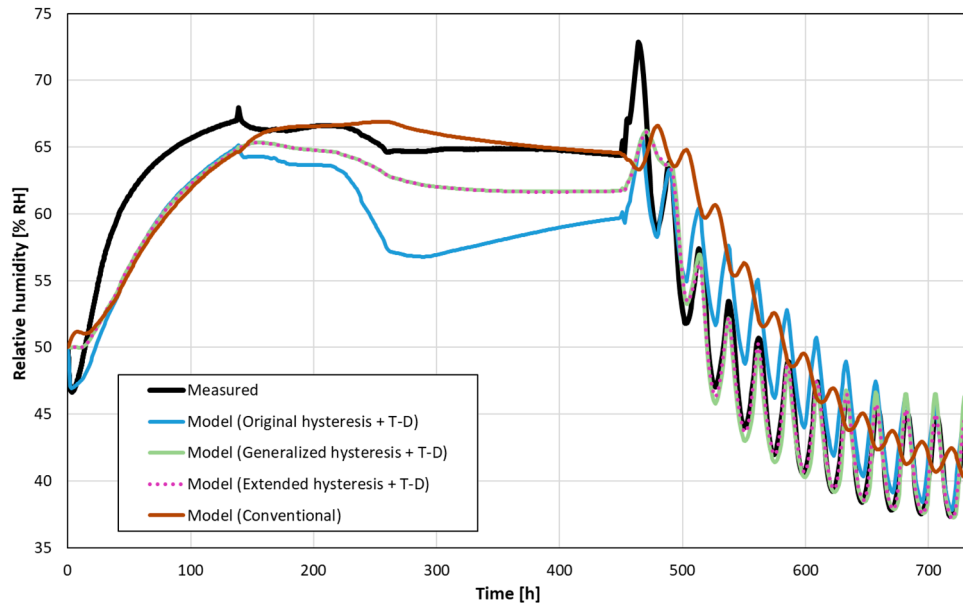
Figure 5. Comparison of relative humidity measurements and simulation results in the RP of test wall 1a (initial relative humidity 50% RH).
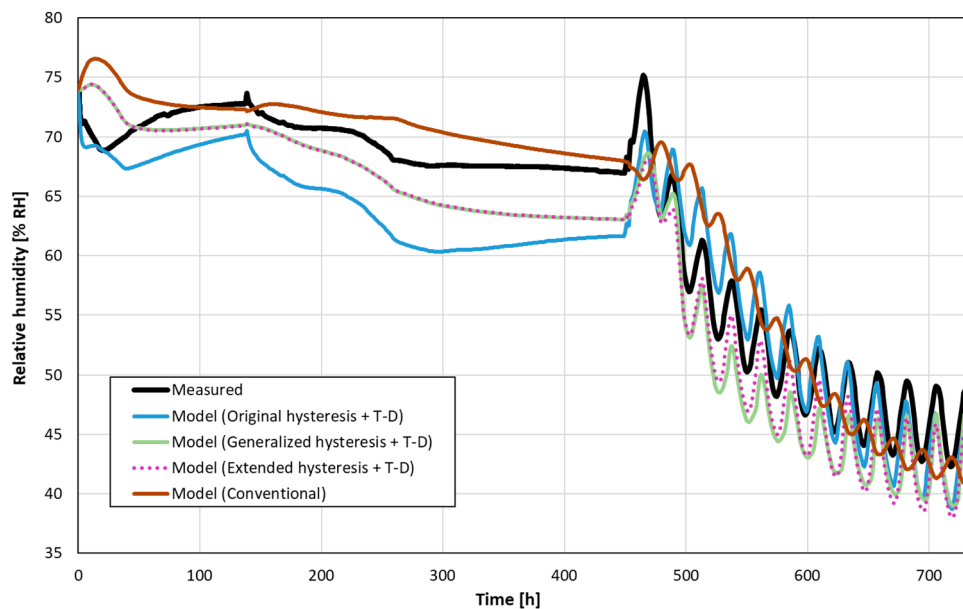

Figure 6. Comparison of relative humidity measurements and simulation results in the RP of test wall 1b (initial relative humidity 74% RH).

according to the adsorption curve. We can see that the generalized and extended models yield practically the same results in moisture content. Interestingly, the original model predicts higher moisture contents especially in test wall 1b, but also lower relative humidities in the same time, i.e. in the autumn and winter phases. The evolutions of the states of moisture in the (φ, u)-coordinate system are compared between different models in Figure 11 where the higher moisture contents can also be seen.

A comparison of results from the hysteresis models, where the temperature-dependence was neglected, and the non-hysteretic (conventional) model, where the temperature-dependence was applied, is shown in Figure 12. We can see that none of these models agree satisfactorily with the measurements in the spring phase. We conclude that when modelling LDF sheathing in a cold climate – i.e. when it experiences dynamic variation in both surrounding temperature and humidity – both
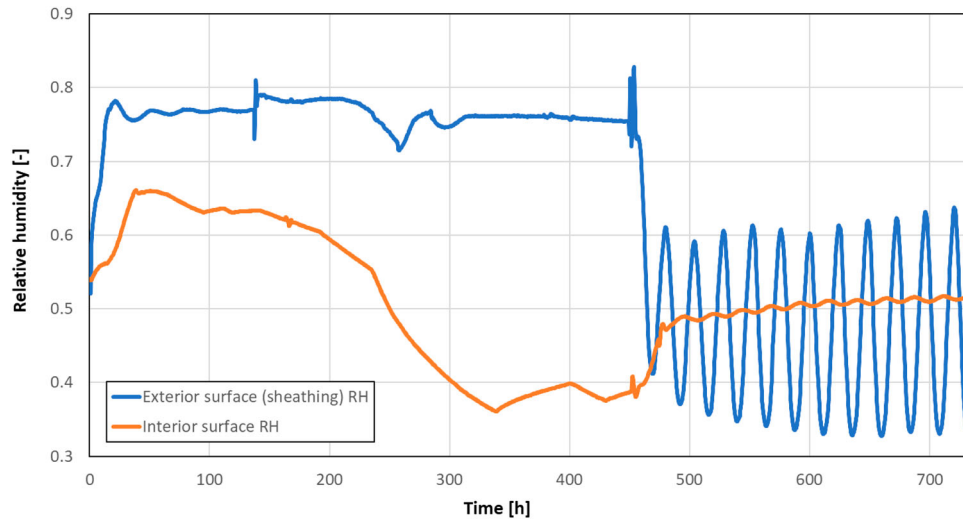
Figure 7. Relative humidity conditions at the boundaries of the models.
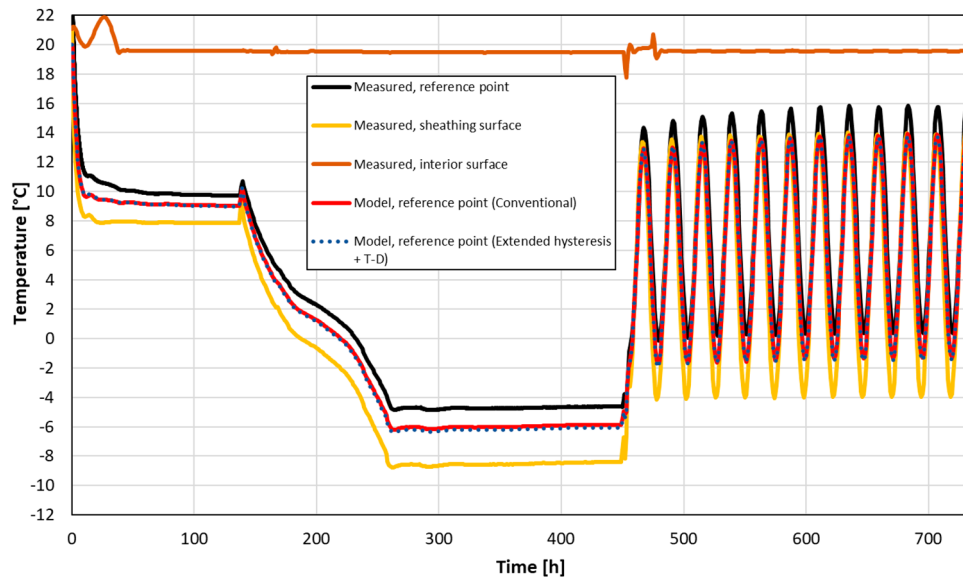

Figure 8. Measured and simulated temperatures in the RP of test wall 1a (initial relative humidity 50% RH).

the hysteresis and temperature-dependence of sorption properties need to be taken into account simultaneously.

4. Discussion

In this research, we carried out sorption isotherm measurements in 20°C and combined the results with measurements in sealed test tubes conditioned in a temperature chamber to construct a temperature-dependent moisture content function for LDF. We applied the results in hygrothermal modelling of the laboratory test assembly, which had the LDF layer as sheathing. The hysteretic sorption characteristics were taken into account with the existing hysteresis model for which the empirical parameters were determined by optimization against the measurements. Some sensitivity analysis was carried

out for the models by varying the values for thermal conductivities and vapour permeabilities, but the effect on the results was minuscule compared to the inclusion of temperature-dependency and hysteresis in the hygrothermal model. Compared to the conventional way of hygrothermal modelling, the new modelling results were clearly improved in the spring phase of the laboratory test, which lasted approximately for a month and where the outer regions of the test assembly experienced diurnal variation in both temperature and humidity.

The temperature-related sorption data applied in the analyses of Zhang et al. (2016) was originally published in 1957 (Kelsey 1957), and the lowest temperature for which the moisture capacity curves were shown was 10°C (Klinki pine). Data was used to formulate the temperature-dependent sorption function, where the
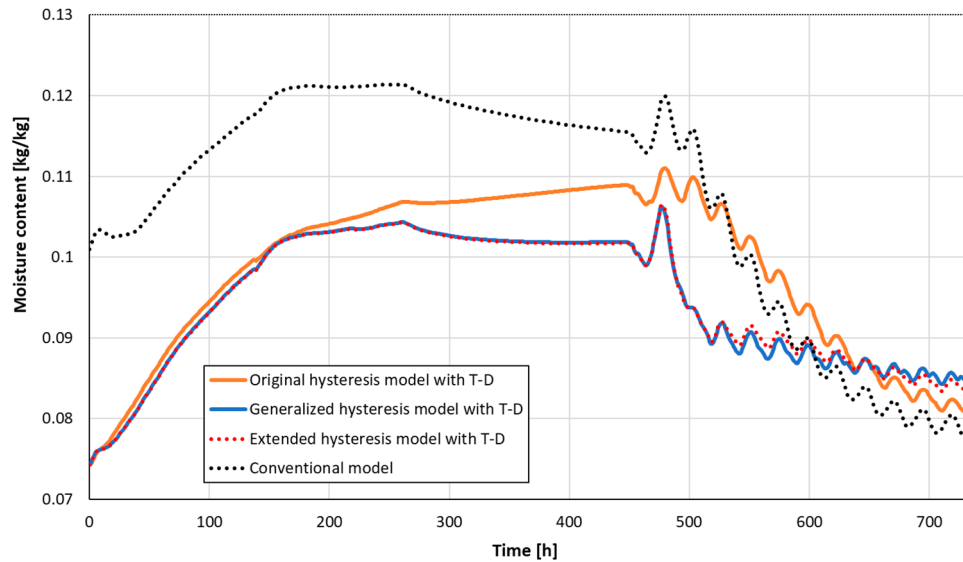
Figure 9. Comparison of LDF moisture content in the RP according to different models (1a, initial relative humidity 50% RH).
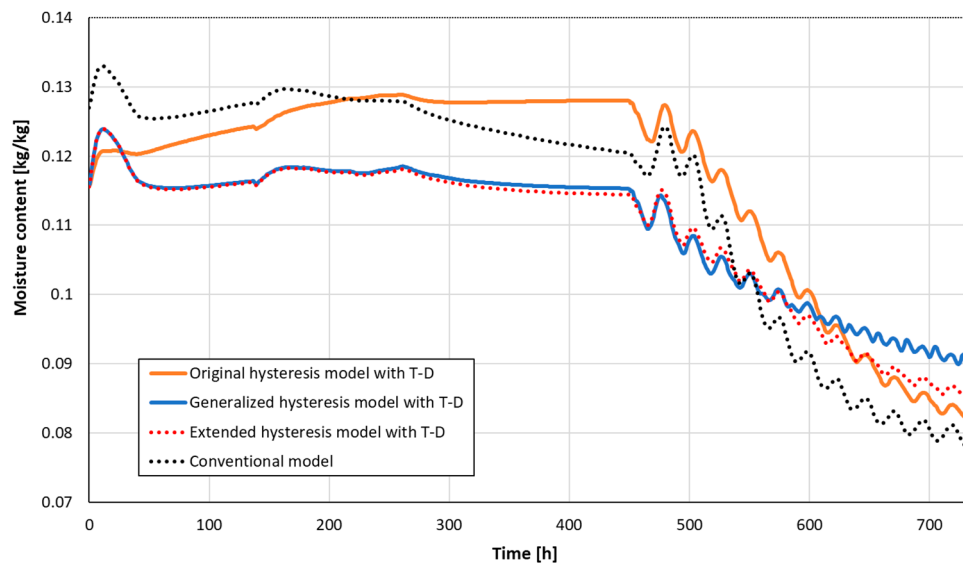

Figure 10. Comparison of LDF moisture content in the RP according to different models (1b, initial relative humidity 74% RH).

effect of temperature was linear, i.e. the moisture capacity always increases when the temperature decreases. We can see from Figure 3 that we could have also used linear interpolation between the data points instead of a second-order polynomial to construct the temperature-dependent data set required in the computations, likely without a significant effect on the results and conclusions. However, contradictory to our measurement results, a theoretical conception can be found from the literature, which implies that the phenomenon called coldness-shrinkage causes moisture capacity to decrease below 0°C (Skaar 1988). For example, the simulations of Rode & Clorius relied on this conception when treating the material data for the simulations (Rode and Clorius 2004). However, the data provided by Hedlin (1967), which was

used by Rode & Clorius among other sources, shows that, e.g, the EMCs of Norway spruce are higher in 3°F (−16°C) than in 10 °F (−12°C) for both adsorption and desorption. As mentioned by Zhang et al., opposing arguments exist in literature on how significant an effect hysteresis has overall in dynamic hygrothermal modelling. Since the moisture capacity has an effect only on the time-derivative terms, temperature-dependence of sorption or hysteresis has no effect in a steady state. Based on their study, Zhang et al. concluded that neglecting temperature-dependency may have significance in some cases when assessing the risk of mould growth with hygrothermal simulations (Zhang et al. 2016). Since the laboratory experiment analysed in this paper was rather short, we cannot yet make any conclusions on this
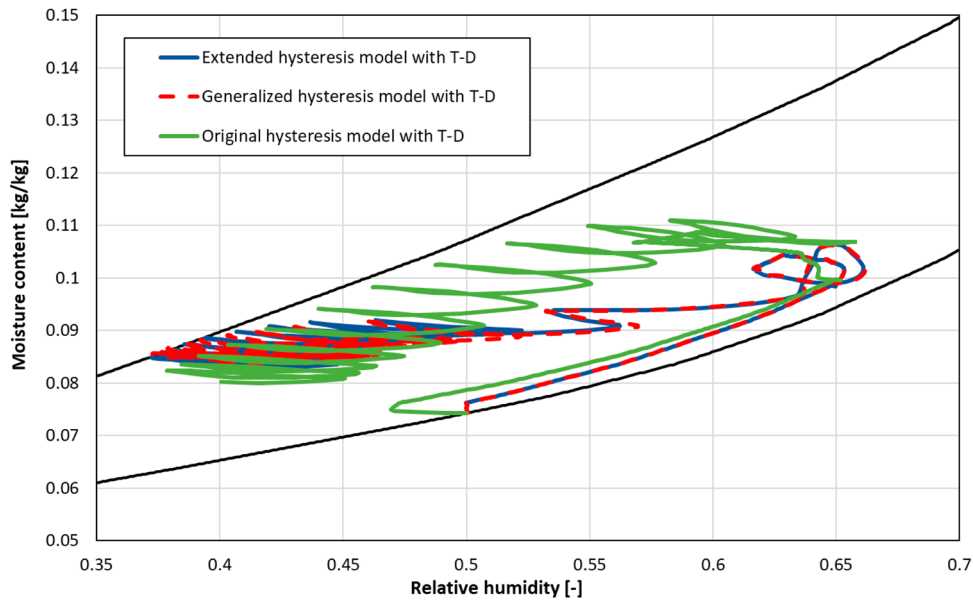
Figure 11. Evolution of the state of moisture in the RP of test wall 1a (initial relative humidity 50% RH) according to the hysteresis models in the (relative humidity, moisture content) – coordinate system. Black lines: Primary sorption isotherms at 20°C.
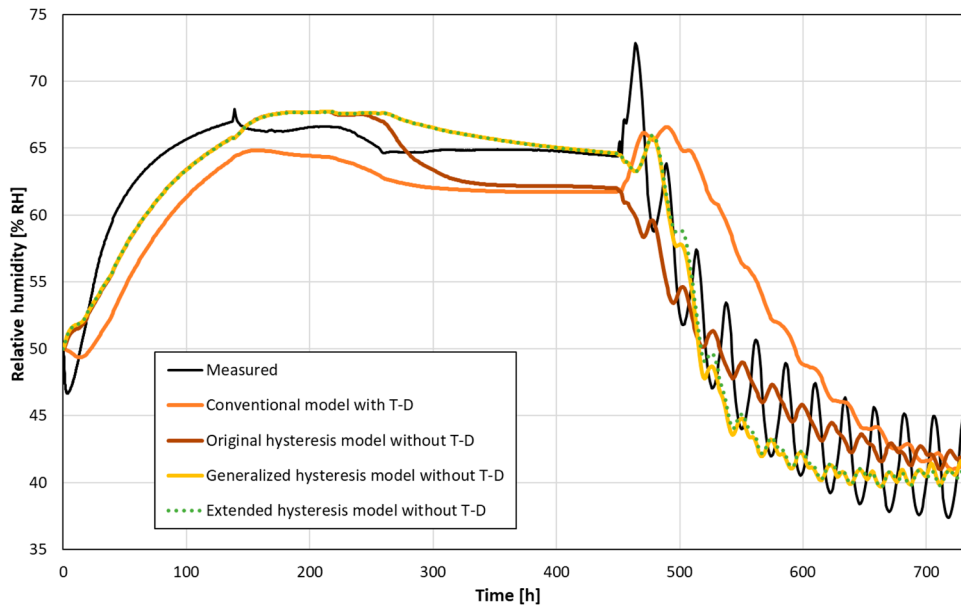

Figure 12. Comparison of simulated results (relative humidity in the RP of test wall 1a) with non-temperature-dependent hysteresis models and temperature-dependent conventional model.

question. However, for further study we are planning a set of long-term analyses of envelope structures in a cold climate, where the results of this paper are utilized. Thybring et al. have pointed out that no current theoretical model can explain the sorption process and its relation to thermal and mechanical phenomena in wood satisfactorily (Thybring, Glass, and Zelinka 2019), which affirms that sorption-related material data should be based on empirical data rather than theoretical models. In consideration of the matters presented above, we think that the significance of the combined effect of hysteresis and

temperature-dependency of sorption in hygrothermal modelling of envelope assemblies is an open question and more experimental and computational research is still needed. The LDF material studied in this paper is manufactured by using the byproducts of different processes of the Finnish wood industry and thereby contains different species (i.e. Norway pine and Picea abies, which cover over 90% of Finland's forests). Although the cellular composition of these two species differ to some degree, we see it as worthwhile to also utilize, with certain assumptions, the temperature-dependence data and

hysteresis parameters provided by this paper for unprocessed structural timber in advanced hygrothermal simulations. Such research could provide us with knowledge on the significance of the combined effect of hysteresis and temperature-dependency of sorption in assessing e.g. mould growth risks in the long term.

Disclosure statement

No potential conflict of interest was reported by the author(s).

Funding

This work was supported by Tampere University.

Data availability statement

The data that support the findings of this study are available from the corresponding author (Petteri Huttunen) upon reasonable request.

List of symbols

ρ density, kg/m^3

C_p specific heat capacity at constant pressure, J/(kg·K)

T temperature, K or °C

t time, s

λ thermal conductivity, W/(m·K)

h_v latent heat of vapourization, J/kg

δ_p water vapour permeability, kg/(m·s·Pa)

φ relative humidity, - or % RH

p_{sat} partial pressure of water at saturation, Pa

w moisture content, kg/m^3

ξ differential moisture capacity, kg/kg or kg/m^3

D_w liquid water transport coefficient, m^2/s

θ auxiliary function, –

ω_i effective hysteresis parameter, –

u moisture content, kg/kg

Δt time step, s

S_d vapour diffusion equivalent air layer thickness, m

μ vapour resistance factor, –

References

Carmeliet, J., M. De Wit, and H. Janssen. 2005. "Hysteresis and Moisture Buffering of Wood." *Proceedings of the Nordic Symposium on Building Physics 2005*, 12–15 June 2005, Reykjavik, Iceland, 2005, 55–62.

Comsol. 2023. *Comsol Multiphysics Documentation*. https://doc.comsol.com/.

Dinwoodie, J. M. 2000. *Timber: Its Nature and Behavior*. 2nd ed. E & Fn Spon, London.

Frandsen, H. L. 2007. *Selected Constitutive Models for Simulating the Hygromechanical Response of Wood*. Department of Civil Engineering, Aalborg University. DCE Thesis No. 10.

Fredriksson, M., and E. E. Thybring. 2018. "Scanning or Desorption Isotherms? Characterising Sorption Hysteresis of Wood." *Cellulose* 25 (8): 4477–4485. https://doi.org/10.1007/s10570-018-1898-9.

Hedlin, C. P. 1967. "Sorption Isotherms of Twelve Woods at Subfreezing Temperatures." *Forest Products Journal* 17 (12): 43–48.

ISO 12571:2021. 2021. *Hygrothermal Performance of Building Materials and Products — Determination of Hygroscopic Sorption Properties*.

Kalamees, T., and J. Vinha. 2003. "Hygrothermal Calculations and Laboratory Tests on Timber-Framed Wall Structures." *Building and Environment* 38 (5): 689–697. https://doi.org/10.1016/S0360-1323(02)00207-X.

Kelsey, K. E. 1957. "The Sorption of Water Vapor by Wood." *Australian Journal of Basic and Applied Science* 8: 42–54.

Künzel, H. M. 1995. "Simultaneous Heat and Moisture Transport in Building Components. One- and Two-Dimensional Calculation Using Simple Parameters." Dissertation. Fraunhofer IRB Verlag Suttgart 1995 (ISBN 3-8167-4103-7).

Laukkarinen, A., and J. Vinha. 2011. "Comparison of Calculated and Measured Values of Wall Assembly Tests Using Delphin 5." 9th Nordic Symposium on Building Physics - NSB 2011. Vol. 1, 155–162.

Lelievre, D., T. Colinart, and P. Glouannec. 2014. "Hygrothermal Behaviour of bio-Based Building Materials Including Hysteresis Effects: Experimental and Numerical Analyses." *Energy and Buildings* 84: 617–627. https://doi.org/10.1016/j.enbuild.2014.09.013.

Rahim, M., A. D. Tran Le, O. Douzane, G. Promis, and T. Langlet. 2016. "Numerical Investigation of the Effect of non-Isotherme Sorption Characteristics on Hygrothermal Behaviour of two bio-Based Building Walls." *Journal of Building Engineering* 7: 264–272. https://doi.org/10.1016/j.jobe.2016.07.003.

Rode, C., and C. O. Clorius. 2004. "Modeling of Moisture Transport in Wood with Hysteresis and Temperature-Dependent Sorption Characteristics." Buildings IX Conference Proceedings. 15 pp.

Rode, C., P. N. Hansen, and K. K. Hansen. 1990. "Combined Heat and Moisture Transfer in Building Constructions." Technical University of Denmark. Byg Rapport No. LFV-214.

Skaar, C. 1988. *Wood-Water Relations. Springer Series in Wood Science*, 283 pp. Berlin, Heidelberg: Springer-Verlag.

Thybring, E., S. Glass, and S. Zelinka. 2019. "Kinetics of Water Vapor Sorption in Wood Cell Walls: State of the Art and Research Needs." *Forests* 10 (8): 704. https://doi.org/10.3390/f10080704.

Vinha, J. 2007. "Hygrothermal Performance of Timber-Framed External Walls in Finnish Climatic Conditions: A Method for Determining the Sufficient Water Vapour Resistance of the Interior Lining of a Wall Assembly." Dissertation. Publication 658, Tampere University of Technology, http://urn.fi/URN:NBN:fi:tty-200903101040 338 pages + 10 app. pages.

Zhang, X., W. Zillig, H. M. Künzel, C. Mitterer, and X. Zhang. 2016, September. "Combined Effects of Sorption Hysteresis and its Temperature Dependency on Wood Materials and Building Enclosures-Part II: Hygrothermal Modeling." *Building and Environment*. *Volume* 106: 181–195. https://doi.org/10.1016/j.buildenv.2016.06.033.